
Learning to Iteratively Improve 3D Representation with 2D Generative Models

Anonymous Author(s)

Abstract

1 Reconstructing three-dimensional (3D) representations from sparse image data is
2 a core task that requires learning to sample plausible 3D models that correspond
3 to 2D conditioning images. Despite numerous proposed frameworks, achieving
4 photorealistic sparse-view 3D reconstructions remains an unresolved challenge,
5 with current methods often producing blurry results on small object-centric scenes
6 that fall short of the fidelity achieved by dense-view 3D reconstruction and 2D
7 generative models. This paper aims to rethink the use of image generative models
8 for 3D reconstruction and introduces a novel framework based on iterative refine-
9 ment. Our approach infers the 3D representation by optimizing it to match images
10 sampled by a 2D generative model, itself conditioned on the current progress of
11 the 3D optimization. To learn this conditional generative model, we design a new
12 training strategy that performs 3D reconstruction using various numbers of views
13 and captures the progress at each optimization timestep. This allows the model
14 to explicitly learn to sample images that are consistent with the current stage of
15 3D reconstruction, supporting sampling of thousands of consistent images during
16 reconstruction. Experiments on a challenging real-world dataset demonstrate com-
17 petitive performance in single-view 3D reconstruction, performing on par with
18 state-of-the-art 3D reconstruction methods based on 2D generative model outputs
19 and dense multiview images.

20 **1 Introduction**

21 Reconstructing a three-dimensional (3D) representation of the physical world from sparse signals,
22 such a two-dimensional (2D) image, is a fundamental task in the fields of computer vision, graphics,
23 and artificial intelligence. Such representations are crucial for applications in augmented and virtual
24 reality (AR/VR) as they allow rendering from novel viewpoints, and in navigation, robotics and AI,
25 as they support reasoning about object extents and the world around us. However, despite the plethora
26 of frameworks proposed in the last decades, the reconstruction of 3D scenes from one or few images
27 remains an unresolved problem.

28 The challenge lies in the inherent ambiguity of the task: multiple 3D scenes can correspond to a
29 single 2D image, and even more possibilities exist for the unbounded space outside the region seen
30 in the image. Consequently, photogrammetry methods, including recent methods based on neural
31 networks [48], which reconstruct a 3D scene using large dataset of images, fail when only few images
32 are available, as they cannot sample plausible content in regions that are unobserved in the input
33 images. More formally, the reconstruction task is probabilistic and generative in nature—its solution
34 is a plausible 3D sample out of many possible ones, requiring learning the model capable of sampling
35 from a posterior probability distribution conditioned on one or more input images.

36 Inspired by the progress of generative models of images and videos, the last decade of 3D research has
37 investigated using neural networks to learn a prior about how 3D scenes should look. However, unlike
38 in 2D datasets that are easy to collect from widely available images on the internet, large datasets
39 of unbounded 3D scenes are infeasible to create. Therefore, the research community is on a quest
40 to find algorithms that learn a prior over the 3D world from only multi-view image datasets, such
41 as ones captured from a consumer camera [61]. Two dominant streams of research have emerged;
42 each, however, produces blurry reconstructions, significantly lagging behind techniques that utilize

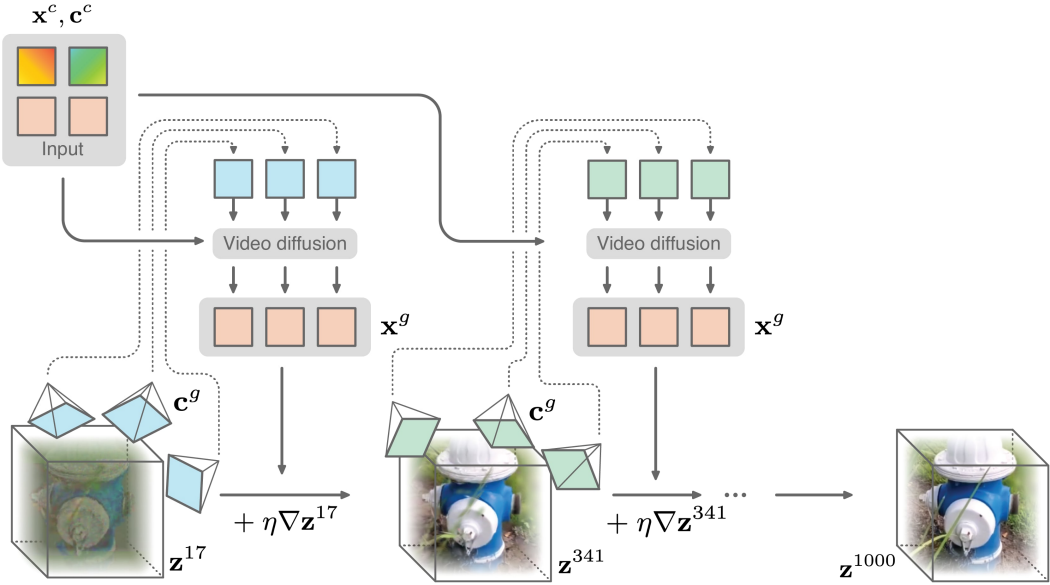


Figure 1: Proposed framework for 3D reconstruction. Given input views and poses, $\mathbf{x}^c, \mathbf{c}^c$, our framework uses generative image model to generate images \mathbf{x}^g at novel viewpoints \mathbf{c}^g , conditioned on 3D representation \mathbf{z}^t at each optimization step t . An optimization step is taken at each iteration, where the gradient $\nabla \mathbf{z}^t$ is computed by rendering representation \mathbf{z}^t to generated image viewpoints \mathbf{c}^g . In contrast to prior works where images are generated in one-shot manner, our approach allows sampling thousands of images over time, each increasingly consistent with each other.

43 dense sets of views, such as Gaussian Splatting, and those for photorealistic 2D image generation,
44 like image diffusion models [6]. Some works have proposed 3D-aware generative models [3, 9, 38]
45 which learn to model 2D images by rendering a 3D representation. These methods hand-engineer
46 differentiable rendering into the probabilistic model, enforcing the model to learn a prior over this 3D
47 representation. However, hand-engineered representations and rendering operators cannot perfectly
48 capture real-world scenes and limits the capacity of the generative model. Some works learn black-box
49 generative models to generate images from novel viewpoints [43, 18], and afterwards use many-view
50 photogrammetry to reconstruct 3D from generated dataset of images. However, for a reconstruction
51 of an unbounded 3D scene, photogrammetry methods require hundreds of images, which current
52 models cannot generate [18]. Moreover, such methods generate images in one shot, often resulting in
53 inconsistencies, which lead to blurry results from the 3D reconstruction stage.

54 In this work, we rethink how to best use image generative models for the task of 3D reconstruction,
55 and introduce a novel framework for sampling a 3D reconstruction given one or few images. Similarly
56 to most recent works, we use general many-view 3D reconstruction methods operating on generated
57 images. However, instead of sampling a dataset of images in one shot, our probabilistic model
58 samples images iteratively, over the course of optimization, each consistent with the current state of
59 the 3D representation. Unlike 3D-aware generative models, our method supports unbounded scenes
60 of unlimited resolution and can integrate any number of conditioning images. Unlike previous 2D
61 generative models, our method can generate thousands of images consistent with each other and
62 with the 3D representation, supporting reconstruction of large scenes. This framework effectively
63 decouples representation from inference, making it scalable and general-purpose [73], allowing it to
64 be used as plug-and-play component on any existing 3D reconstruction pipeline, such as Gaussian
65 Splatting [34] or NeRFs [48]. In our experiments, we instantiate this framework using Gaussian splats
66 as the representation and video diffusion as the generative model; we demonstrate state-of-the-art
67 performance in sparse view 3D reconstruction, surpassing competing frameworks of latent variable
68 generative models and 3D reconstruction from 2D generative model outputs.

69 2 Prior Methods

70 In this section, we analyse various frameworks that have been proposed to reconstruct 3D scene
71 representations from images. We first (Sec. 2.1) summarise various methods for representing and

72 rendering the 3D world, which can be inverted to reconstruct from a dense set of images. We then
 73 discuss (Sec. 2.2) generative models which can sample 3D scenes given sparse images and then
 74 review generative 3D models that learn to sample 3D representations whilst learning from 2D images.

75 **2.1 3D Representation and Rendering**

76 Computer graphics has developed methods for representing the physical 3D world and simulating the
 77 image formation process via rendering [32], enabling generation of realistic images. The core idea of
 78 inverse graphics is that given a dataset D of images and their poses $\{(\mathbf{x}^i, \mathbf{c}^i) \mid i = 0, \dots, N\}$, the
 79 process of rendering can be “inverted” to infer a 3D representation \mathbf{z} that generated the images. This
 80 is achieved by optimization that minimizes reconstruction a loss where gradients with respect to the
 81 3D representation $\nabla \mathbf{z}$ are calculated using a differentiable rendering function:

```

82 D ← {(\mathbf{x}^i, \mathbf{c}^i) \mid i = 0, \dots, N}
83 def reconstruct(D, T, render(), \mathbf{z}^0):
84     for t in range(T):
85         \mathbf{x}^g, \mathbf{c}^g ← random.choice(D)
86         \nabla \mathbf{z}^t ← render(\mathbf{z}^t, \mathbf{c}^g).loss(\mathbf{x}^g).grad
87         \mathbf{z}^{t+1} ← \mathbf{z}^t + \eta \nabla \mathbf{z}^t
88     return \mathbf{z}^T
89

```

91 Under certain assumptions, such as a large number of input images N , such inference process
 92 results in a good 3D representation that can then be rendered to novel views. Over the years
 93 many representations and rendering algorithms have been proposed, the most popular being surface
 94 representations (such as distance fields and polygon meshes) that can be rendered to images by
 95 rasterization or path tracing. Since meshes are difficult to optimize using gradient descent due to non-
 96 local gradients, neural radiance fields (NeRFs) [48] have been introduced, which represent a volume
 97 with a neural network. More recent works, such as iNGP [51] and 3D Gaussian Splatting [34, 39],
 98 have focused on increasing the speed of training and rendering to real-time. Another direction is
 99 aimed to acquire physically meaningful representations [55]. However, a core limiting assumption is
 100 access to large amount of training images (e.g. capturing every side of the object), typically requiring
 101 $N > 100$ for a single room and $N > 1000$ for multi-room scenes. Consequently, when such an
 102 amount of images is not feasible to acquire in practice, these methods produce floating artifacts and
 103 empty volumes in under-sampled regions of 3D space. Some methods aim to fix reconstruction errors
 104 using regularizers on depth, normal, or colors, or by discriminators and image generative models
 105 [54, 63, 44, 31]. However, these approaches already assume access to a fully reconstructed 3D model.

106 **2.2 Generative Models**

107 Generative models learn to sample from the complex distribution of their training data. Various
 108 families have been proposed including Generative Adversarial Networks (GAN) [19], Variational
 109 Autoencoders (VAE) [62, 36], autoregressive models [81, 80, 60] and Independent Component
 110 Analysis (ICA) [30]. Recent success in high-dimensional data, such as images [64], videos and
 111 sound, have been achieved by score-based generative models [69, 71, 70], particularly denoising
 112 diffusion probabilistic models (DDPM) [26, 72]. These learn to estimate the gradient $\nabla \mathbf{z}^t$ of the
 113 log probability $p(\mathbf{z}, t)$ (termed “score”) with respect to the data at a noise scale t . Inspired by their
 114 success in other modalities, DDPMs have been adopted to sample 3D representations by learning
 115 from datasets of ground-truth 3D representations [11, 14], such as pointclouds [46, 79], Neural Fields
 116 [5, 50, 29, 40, 12, 84, 35, 68, 21, 33, 20] or 3D Gaussians [89, 49]. At test-time, these methods
 117 support conditioning on input views \mathbf{x}^c and poses \mathbf{c}^c , and sampling a plausible 3D reconstruction \mathbf{z} :

```

118 def reconstruct(\mathbf{x}^c, \mathbf{c}^c, T, P_\theta, \sigma):
119     \mathbf{z}^0 ← random()
120     for t in range(T):
121         \nabla \mathbf{z}^t ← P_\theta(\mathbf{z}^{t+1} \mid \mathbf{z}^t, \mathbf{x}^c, \mathbf{c}^c).sample()
122         \mathbf{z}^{t+1} ← \alpha^t \mathbf{z}^t + \eta^t \nabla \mathbf{z}^t
123     return \mathbf{z}^T
124

```

126 We similarly aim to perform flow matching between randomly sampled 3D representations and
 127 empirical distribution of 3D representations. However, unlike 2D images, large datasets of highly-
 128 realistic and large-scale 3D scenes are challenging or even infeasible to create. Therefore, we propose
 129 a method that learns to sample 3D scenes whilst learning from widely available 2D image datasets.

130 **Structure-in.** Some methods aim to learn to sample latent 3D representations whilst learning to
 131 generate 2D images. These methods typically have a 3D representation inside their architecture,
 132 hence often denoted as “3D-aware” or “structure-in”, as the 3D representation and rendering are
 133 hand-engineered inside the network. These models define a likelihood over images by sampling a
 134 latent variable corresponding to a 3D representation and then rendering it to an image. For example,
 135 3D-aware diffusion [3] learns to denoise image via underlying 3D representation, 3D-aware VAEs
 136 learn a latent variable model where latent variable is a 3D representation [38, 23, 25, 1, 24] and
 137 3D-aware GANs learn a generator that generates images by first generating a 3D representation
 138 [53, 66, 9, 15, 52, 16]. This framework has been extended to in-the-wild datasets [2, 87, 45, 28, 74,
 139 78, 27, 8]. However, the core limitation of these models is that 3D representation and rendering have
 140 to be hand-engineered into the model. This restricts the flexibility and capacity of the model, as the
 141 representations are of limited flexibility and the rendering operation is only approximate. For example,
 142 current state-of-the-art generative methods use representations having a limited number of parameters,
 143 such as voxel grids, triplanes, or image-supported features. Furthermore, their renderers only consider
 144 the final bounce of light from one surface to the camera, e.g. without modelling reflections. Some
 145 approaches replace hand-engineered rendering by a learnt “neural” renderer [17, 10], however at the
 146 cost of losing the 3D representation that is needed in many applications.

147 **Structure-out.** Instead of hand-engineering the 3D representation and rendering inside the gener-
 148 ative model, some approaches try to extract 3D structure from 2D images generated by black-box
 149 generative models. The most straightforward approach is to generate a dataset of images and poses
 150 $D = \{(\mathbf{x}^i, \mathbf{c}^i) \mid i = 0, \dots, N\}$ using a generative video model and then run an optimization-based
 151 3D reconstruction method as described in Sec 2.1. This has the benefit that advancements in graphics
 152 can be utilised out-of-the box, e.g. by using unconstrained and flexible 3D representations with
 153 reflection-aware rendering, which avoids hand-engineering generative image models, and allows
 154 flexible and powerful architectures trained on large amounts of 2D datasets. Most recent works
 155 [22, 82, 18, 86, 47, 90, 43, 77, 45, 37, 42, 75, 6] use image diffusion models fine-tuned with camera-
 156 pose and then generate a dataset of 2D images from which 3D is reconstructed. However, the classic
 157 3D reconstruction methods assume access to large amount of 3D consistent images N . In contrast,
 158 current approaches generate images that are slightly inconsistent, both due to limited performance of
 159 generative models and due to camera pose conditioning being incorrect. Consequently, this leads
 160 the 3D reconstruction method to “average out” these inconsistencies, resulting in blurry regions.
 161 Another problem is that generating hundreds or thousands of images is not possible with current
 162 multi-view generative models. Instead, current approaches generate small sets of images conditionally
 163 independently from each other, which results in inconsistent 3D scenes even assuming access to a
 164 perfect generative model. A concurrent work [18] generates images in sets of 8, first generating a set
 165 of anchor frames and then autoregressively generating the rest; it relies on ad-hoc techniques, such as
 166 using LPIPS loss [86, 18] to be invariant to inconsistent generated images. Consequently, current
 167 methods are limited to small and bounded object-centric scenes where small number of images suffice.
 168 In this work, we use generative image models to generate thousands of consistent images by explicitly
 169 training the model to output images that are consistent with previous generations.

170 3 Method

171 Our method tackles the problem of reconstructing a 3D representation from a small number of
 172 input images. The proposed framework modifies only one line in the classical 3D reconstruction
 173 pipeline (Sec. 2.1) – instead of using dataset of images and poses, our framework samples images \mathbf{x}^g
 174 iteratively throughout the optimization process. At each optimization step t , images \mathbf{x}^g are sampled
 175 from a learnt probabilistic generative model P_θ conditioned on the current stage of reconstruction \mathbf{z}^t
 176 and input (conditioning) images and poses $\mathbf{x}^c, \mathbf{c}^c$. Then, a gradient with respect to the representation
 177 $\nabla \mathbf{z}^t$ is computed by rendering representation to images:

```

178 def reconstruct( $\mathbf{x}^c, \mathbf{c}^c, T, P_\theta, \text{render}()$ ,  $\mathbf{z}^0$ ):
179     for  $t$  in  $\text{range}(T)$ :
180          $\mathbf{c}^g \leftarrow P_\lambda(\mathbf{c}^g \mid \mathbf{c}^c).\text{sample}()$ 
181          $\mathbf{x}^g \leftarrow P_\theta(\mathbf{x}^g \mid \mathbf{z}^t, \mathbf{x}^c, \mathbf{c}^g).\text{sample}()$ 
182          $\nabla \mathbf{z}^t \leftarrow \text{render}(\mathbf{z}^t, \mathbf{c}^g).\text{loss}(\mathbf{x}^g).\text{grad}$ 
183          $\mathbf{z}^{t+1} \leftarrow \mathbf{z}^t + \eta \nabla \mathbf{z}^t$ 
184     return  $\mathbf{z}^T$ 
185

```

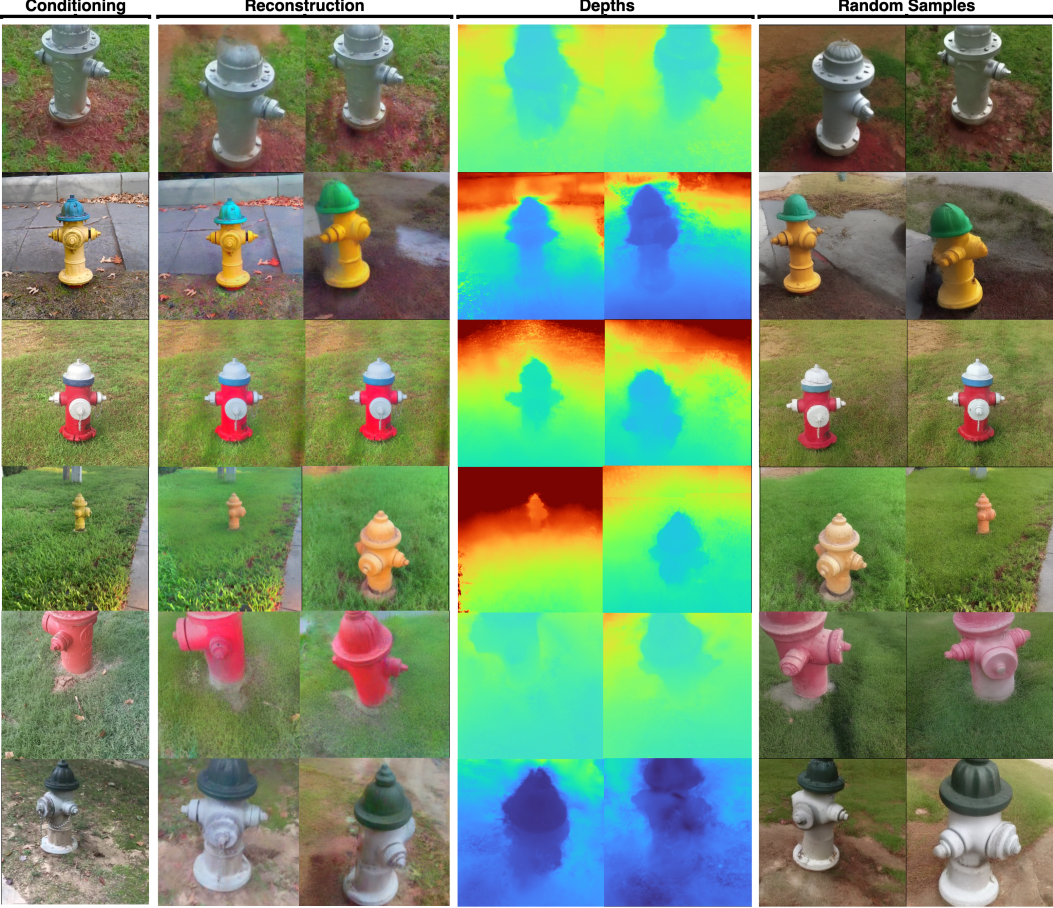


Figure 2: Qualitative results from our model on 3D reconstruction from a single image (first three rows) and six images (next three rows). The leftmost column shows the input (conditioning), followed by two novel views rendered from the reconstructed 3D representation and their corresponding depth maps. The final columns present samples from our generative model at an early stage t of optimization, illustrating its ability to generate diverse yet consistent images, each pushing the 3D representation closer to the true posterior sample.

187 Note that this framework separates 3D representation and rendering from the generative image
 188 model, allowing out-of-the-box use of advancements in graphics (e.g. fast optimization and real-time
 189 rendering of 3D Gaussian Splatting [34, 39]) and unconstrained architecture of generative model
 190 (e.g. diffusion or flow-based models). Importantly, at each step, the generative model is conditioned
 191 on the current stage of reconstruction \mathbf{z}^i , allowing to sample images that are consistent with the
 192 3D scene and previous generations $t-1, t-2, \dots, 0$. Note that we do *not* maximize likelihood,
 193 i.e., $P_\theta(\mathbf{x}^g \mid \mathbf{z}^t, \mathbf{x}^c, \mathbf{c}^g)$.likelihood(render($\mathbf{z}^t, \mathbf{c}^g$)), as this would lead to mode-seeking optimization
 194 behavior, akin to score-distillation sampling [58, 85, 83, 76, 41], resulting in poor reconstruction
 195 quality when the conditioning datapoint does not reside near the modes of the distribution. In this
 196 section, we describe this framework by providing details on the generative model (Sec. 3.1), how it is
 197 conditioned on current stage of reconstruction (Sec. 3.3) and input (Sec. 3.4), model training (Sec.
 198 3.5), and representation and rendering (Sec. 3.6).

199 **3.1 Generative Model**

200 At each optimization step t , we use a learnt probabilistic model to sample images that are consistent
 201 with both input conditioning and previously generated images. Specifically, the probabilistic model
 202 $P_\theta(\mathbf{x}^g \mid \mathbf{z}^t, \mathbf{x}^c, \mathbf{c}^g)$ samples images \mathbf{x}^g at specific poses \mathbf{c}^g , conditioned on the current stage of
 203 reconstruction \mathbf{z}^t . The generation poses \mathbf{c}^g are sampled in such way that minimizes the prediction
 204 entropy of the autoregressive chain (see Sec. 3.2). For the generative model, we adopt the framework
 205 of Latent Video Diffusion Models (LVDM) [64, 7, 57]. LVDMs employ Denoising Diffusion

206 Probabilistic Models [69, 26, 71] to generate latent variables, which are then decoded into multi-view
 207 images. For simplicity, latent representations are omitted in figures. During training, the model is
 208 trained to denoise target images \mathbf{x}^g , conditioned on target camera poses \mathbf{c}^g , conditioning input images
 209 \mathbf{x}^c , and the current stage of 3D reconstruction \mathbf{z}^t . The input to the denoising model consists of noisy
 210 video latents \mathbf{x}^g with dimensions $[G, C, H, W]$, where G is the number of views, C is the number
 211 of channels, and H and W are the height and width of the image latents. The denoising diffusion
 212 model, parameterized by θ , is trained to predict the denoised latents from the noisy latents. During
 213 optimization, to compute the loss (as shown in line 7 of the pseudocode), we use images sampled
 214 from the trained posterior distribution, i.e. $\mathbf{x}^g \leftarrow P_\theta(\mathbf{x}^g \mid \mathbf{z}^t, \mathbf{x}^c, \mathbf{c}^g).\text{sample}()$.

215 3.2 Autoregressive Generation with Uncertainty-Guided Ordering

216 The camera poses where new images are being generated are sampled from $P_\lambda(\mathbf{c}^g \mid \mathbf{c}^c)$, which we
 217 have a control over. We observed that the choice of P_λ has a profound effect on the faithfulness of the
 218 generated images to the conditioning input as well as numerical reconstruction results. We observed
 219 that a naive choice of P_λ , e.g. sampling a starting point randomly around the object as in previous
 220 one-shot works, leads to query poses that are far from previously generated images or from input
 221 poses, where P_θ struggles to generate consistent images. In contrast, we found that P_θ can easily
 222 generate consistent images that are close to previous generations. Therefore, we discovered that the
 223 optimal ordering strategy is to query views that contain the least uncertainty, i.e. would exhibit only
 224 small variation in generations. Thus, we prefer views near to previous generations as opposed to
 225 views of the opposite side of the input image which contain a lot of uncertainty in unobserved regions.
 226 More formally, we aim for an ordering $x_1 \rightarrow x_2 \rightarrow x_3$ of view subsets x_i such that overall entropy is
 227 minimized:

$$H(\mathbf{x}) = H(x_1) + H(x_2 \mid x_1) + H(x_3 \mid x_1, x_2) \quad (1)$$

228 In practice, we first generate various videos (simulating similar camera motions as in the training
 229 data) around the input poses. These are then gradually expanded and the process repeats.

230 3.3 Conditioning on Current 3D Representation

231 We condition generative model P_θ on the current stage of 3D reconstruction \mathbf{z}^t to allow learning to
 232 generate images that are consistent with previously generated images. We achieve this by rendering
 233 3D representation (e.g. partially reconstructed 3D Gaussians) \mathbf{z}^t to the same viewpoints as images to
 234 be generated \mathbf{x}^g and encoding them with the latent diffusion's VAE to get another set of latents. As
 235 these latents are of the same dimensions, we concatenate them as extra channels with noisy latents
 236 and feed them together to the denoising U-Net. We found that such conditioning on current stage of
 237 reconstruction provides the model with a rich signal about previously generated images that were used
 238 for the reconstruction, as the 3D scene is seen from multiple viewpoints. Furthermore, conditioning
 239 our model on renderings provides rich information about camera extrinsics and intrinsics.

240 3.4 Conditioning on Input Images and Poses

241 We condition the generative model on input images and poses. Previous methods have utilized CLIP
 242 conditioning, which leverages features from a large pretrained model optimized for image-to-text
 243 matching [59]. While these features are semantically rich, they may lack detailed information about
 244 high-frequency scene elements, such as precise object shapes and textures. To address this, we
 245 additionally condition the model on DINOv2 features [56], which extract 16x16 spatial tokens and a
 246 global token. However, using all tokens directly is computationally expensive. Therefore, we pool
 247 the 256 spatial tokens into a single token and concatenate it with the global DINO token before
 248 combining them with CLIP embeddings. During training, we condition on a variable number of input
 249 images, allowing the denoising U-Net to cross-attend over these tokens.

250 The model must also understand the relationship between input views and the views it needs to
 251 generate. To achieve this, we add camera pose embeddings and sum them with the DINOv2 features.
 252 To avoid providing duplicate pose information to the generative model, the conditioning poses \mathbf{c}^g
 253 are made relative to the first generated image—i.e., the images provided to the generative model are
 254 always assumed to start at an identity pose. We then perform positional embedding of camera poses
 255 and sum them with other tokens, enabling the U-Net to cross-attend to image tokens based on their
 256 poses.

257 Note that by retaining the classical 3D reconstruction, our framework naturally supports another
 258 pathway for conditioning on an arbitrary number of images, as we can pass them as additional images
 259 to be reconstructed. This is a capability that “structure-in” methods cannot easily achieve (Sec. 2.2).

260 **3.5 Training for Iterative Reconstruction**

261 We use 2D video datasets to train our probabilistic model. However, using 2D image datasets
 262 directly for training is not feasible as our model requires conditioning on the reconstruction \mathbf{z}^t at
 263 optimization step t . Therefore, we construct a dataset by performing classical 3D reconstruction (e.g.
 264 Gaussian Splatting or NeRF as in Sec. 2.1) from varying numbers of input images and rendering
 265 these reconstructions along provided camera trajectories to track optimization progress. For each
 266 scene, we randomly sample the number of input images C from an exponential distribution, favoring
 267 smaller numbers of input images over larger ones. We track the optimization process by rendering the
 268 optimized 3D model every 100 steps across all provided camera trajectories. This results in a dataset
 269 comprising $(\mathbf{x}^c, \mathbf{c}^c, \mathbf{z}^t)$, where t ranges from 0 to 30,000 in increments of 100 steps. Each \mathbf{z}^t is
 270 represented as rendered (latent) images at specific poses. During the training of the LVDM U-Net, we
 271 sample input conditioning images, \mathbf{x}^c , and \mathbf{z}^t (latent images rendered to poses \mathbf{c}^g), training the model
 272 to denoise \mathbf{x}^g at poses \mathbf{c}^g . This unrolled iterative training approach is substantially different from
 273 other models, which either train in a one-shot manner $p(\mathbf{x}^g | \mathbf{c}^c, \mathbf{x}^c)$ [18] or perform super-resolution
 274 of images [67].

275 **Preventing Divergence.** We noticed that during sampling, diffusion model can diverge and generate
 276 saturated, toyish-looking images. We speculate that this is due to conditioning becoming out-of-
 277 distribution than seen during training. Specifically, during training, model sees 3D reconstruction
 278 from sparse ground-truth images rather than model’s own samples. To address this, we add Gaussian
 279 noise to conditioning images during both training and test time. This has the effect of bringing test
 280 and training distributions closer. Furthermore, we use classifier-free with a guidance scale < 1 to
 281 guide the samples towards 3D-unconditional model.

282 **3.6 3D Representation and Rendering**

283 Our sampling procedure aligns closely with standard 3D reconstruction methods, as outlined in
 284 Section 3. This allows us to leverage recent advancements in 3D scene representations and rendering
 285 techniques. We employ Gaussian splatting as the 3D representation [34], incorporating enhancements
 286 from [13]. For the loss function, we utilize both Mean Squared Error (MSE) and Learned Perceptual
 287 Image Patch Similarity (LPIPS).

Table 1: Quantitative comparison on 3D reconstruction. Our approach outperforms prior frameworks
 across nearly all metrics, except compared to CAT3D and ReconFusion, which are not publicly
 available and were evaluated on all categories of CO3D.

	1-view			6-view		
	PSNR \uparrow	SSIM \uparrow	LPIPS \downarrow	PSNR \uparrow	SSIM \uparrow	LPIPS \downarrow
Ours	16.23	0.423	0.501	20.06	0.531	0.360
Ablation: one-shot	15.48	0.417	0.486	19.12	0.535	0.363
Ablation: MEO	15.39	0.404	0.601	17.98	0.371	0.540
Ablation: noisy conditioning	12.84	0.108	0.695	16.99	0.441	0.446
GSplatting [34]	14.89	0.399	0.504	19.41	0.298	0.637
GIBR \dagger [2]	16.07	0.329	0.456	20.22	0.571	0.283
VD \dagger [74]	13.18	0.144	0.714	-	-	-
PixelNeRF \dagger [88]	15.06	0.278	0.615	16.86	0.366	0.545
RD \dagger [3]	15.70	0.317	0.598	18.60	0.399	0.533
SparseFusion \dagger [91]	12.06	-	0.630	-	-	-
ReconFusion* [86]	-	-	-	21.84	0.714	0.342
CAT3D* [18]	-	-	-	22.79	0.726	0.292
ZeroNVS* [65]	-	-	-	19.72	0.627	0.515
Zip-NeRF* [4]	-	-	-	14.48	0.497	0.617

288 **4 Experiments**

289 We conduct experiments on the CO3D dataset [61], which includes camera pose annotations, showing
 290 results on the hydrant class as in prior works [74]. Our evaluation centers on the task of sparse
 291 view 3D reconstruction, where we benchmark our method against several existing frameworks and
 292 ablations of our own approach.

293 In our experiments, we provide models with varying numbers of input frames—specifically 1 or 6
294 frames—to predict the 3D scene. The reconstructed scenes are then rendered from all viewpoints in
295 the original video, and the quality of reconstruction is assessed by comparing the rendered images
296 with ground-truth images. As metrics we use Peak Signal-to-Noise Ratio (PSNR), Learned Perceptual
297 Image Patch Similarity (LPIPS), and Structural Similarity Index (SSIM). Since 3D reconstruction
298 from sparse images is probabilistic in nature, we follow baseline works and draw multiple samples
299 from the model, taking the best-performing sample. Our method is compared against state-of-the-art
300 structure-in frameworks, including GIBR [2], RenderDiffusion [3], pixelNeRF [88], and SparseFusion
301 [91]. Additionally, we evaluate our approach against one-shot generation methods, referencing results
302 from [86, 18, 65]. Since these one-shot methods do not provide open-source code or compatible
303 evaluation pipelines, we cite the numbers directly from their papers. As such, they are included
304 primarily for broader context, and are not strictly comparable to our hydrant-only evaluation protocol.
305 We further ablate our model to demonstrate the advantages of our iterative approach over one-shot
306 methods, and highlighting the impact of autoregressive generation with Uncertainty-Guided Ordering
307 (Sec. 3.2). Lastly, we compare our generative approach to the classical fitting of Gaussian splatting
308 [34], underscoring that it fails in our sparse-view setting.

309 4.1 Sparse-View 3D Reconstruction

310 Table 1 presents quantitative results on sparse view 3D reconstruction. Each method is provided with
311 N input images and their corresponding camera poses, and the reconstructed 3D representation is
312 evaluated by rendering novel views. We follow prior work in considering two levels of difficulty:
313 $N = 6$ and $N = 1$. Our model outperforms most prior approaches across key metrics. In the more
314 challenging single-image 3D reconstruction task, as measured by PSNR and SSIM, our method
315 surpasses the state-of-the-art GIBR [2], which is explicitly trained for novel view prediction and
316 thus less general than ours. For 6-view 3D reconstruction, our method remains highly competitive,
317 achieving strong performance across all three metrics. The main exceptions are GIBR, which performs
318 slightly better, and CAT3D [18]. However, CAT3D is not publicly available, and its evaluation is
319 based on all categories of CO3D rather than the more challenging outdoor hydrant class used in our
320 benchmarks. Consequently, direct comparison may not fully reflect relative performance.

321 4.2 Ablations

322 We conduct ablation studies to analyze the key technical contributions of our framework, specifically
323 iterative generation, 3D conditioning, and Uncertainty-Guided Ordering, demonstrating benefits of
324 each in Table 1.

325 **One-shot vs Iterative.** During training, our probabilistic model learns to generate images at novel
326 views given as input a conditioning image and its camera pose as well as a 3D representation. At
327 test-time, we can use our generative model to generate a large dataset of images, similarly to one-shot
328 approaches, such as CAT3D [18], ablating our iterative approach. In Table 1, we performed a
329 quantitative ablation study, when the iterative approach is replaced with one-shot generation of the
330 multi-view images, when other components are kept the same (e.g. Uncertainty-Guided Ordering).
331 We see that such approach performs significantly worse than the iterative approach. Qualitatively, we
332 see that images generated by the one-shot approach are highly inconsistent, in extreme cases, even
333 changing the shape of the hydrant, which results in a blurry 3D reconstruction. In contrast, though
334 our iterative approach may sample inconsistent results initially, it later converges on one particular
335 3D sample, leading to a sharp and detailed 3D reconstruction.

336 **Ablating Conditioning Noising.** To evaluate the impact of adding Gaussian noise to conditioning
337 images, we conduct an ablation experiment with this component removed. Without noising, the
338 conditioning images rendered from the 3D representation remain unaltered. Table 1 (“Ablation: noisy
339 conditioning”) shows that this leads to a noticeable drop in performance, suggesting that noising
340 helps bridge the distribution gap between training and inference, leading to more stable and realistic
341 generations.

342 **Uncertainty-Guided Ordering.** The query camera poses where new images are generated is
343 sampled from $P_\lambda(\mathbf{c}^g \mid \mathbf{c}^c)$, which in our case, samples camera poses such that the overall entropy of
344 generations is minimized (Sec. 3.2). To study the effect of such design, we ablate this component,
345 replacing it with random sampling around the object (matching prior works). In Table 1, we show
346 quantitative results (“Ablation: UGO”), observing that the model with Uncertainty-Guided Ordering
347 achieves significantly better results across all metrics.

348 **References**

349 [1] T. Anciukevicius, P. Fox-Roberts, E. Rosten, and P. Henderson. Unsupervised causal generative
350 understanding of images. *Advances in Neural Information Processing Systems*, 35:37037–37054,
351 2022.

352 [2] T. Anciukevičius, F. Manhardt, F. Tombari, and P. Henderson. Denoising diffusion via image-
353 based rendering. In *The Twelfth International Conference on Learning Representations*, 2024.

354 [3] T. Anciukevičius, Z. Xu, M. Fisher, P. Henderson, H. Bilen, N. J. Mitra, and P. Guerrero. Ren-
355 derdiffusion: Image diffusion for 3d reconstruction, inpainting and generation. In *Proceedings*
356 *of the IEEE/CVF Conference on Computer Vision and Pattern Recognition (CVPR)*, pages
357 12608–12618, June 2023.

358 [4] J. T. Barron, B. Mildenhall, D. Verbin, P. P. Srinivasan, and P. Hedman. Zip-nerf: Anti-aliased
359 grid-based neural radiance fields. *ICCV*, 2023.

360 [5] M. Á. Bautista, P. Guo, S. Abnar, W. Talbott, A. T. Toshev, Z. Chen, L. Dinh, S. Zhai, H. Goh,
361 D. Ulbricht, A. Dehghan, and J. M. Susskind. GAUDI: A neural architect for immersive 3d
362 scene generation. In A. H. Oh, A. Agarwal, D. Belgrave, and K. Cho, editors, *Advances in*
363 *Neural Information Processing Systems*, 2022.

364 [6] A. Blattmann, T. Dockhorn, S. Kulal, D. Mendelevitch, M. Kilian, D. Lorenz, Y. Levi, Z. English,
365 V. Voleti, A. Letts, V. Jampani, and R. Rombach. Stable video diffusion: Scaling latent video
366 diffusion models to large datasets. *CoRR*, abs/2311.15127, 2023.

367 [7] A. Blattmann, R. Rombach, H. Ling, T. Dockhorn, S. W. Kim, S. Fidler, and K. Kreis. Align
368 your latents: High-resolution video synthesis with latent diffusion models. In *IEEE Conference*
369 *on Computer Vision and Pattern Recognition (CVPR)*, 2023.

370 [8] A. Cao, J. Johnson, A. Vedaldi, and D. Novotny. Lightplane: Highly-scalable components for
371 neural 3d fields. *ArXiv*, 2024.

372 [9] E. R. Chan, C. Z. Lin, M. A. Chan, K. Nagano, B. Pan, S. D. Mello, O. Gallo, L. Guibas,
373 J. Tremblay, S. Khamis, T. Karras, and G. Wetzstein. Efficient geometry-aware 3D generative
374 adversarial networks. In *CVPR*, 2022.

375 [10] E. R. Chan, K. Nagano, J. J. Park, M. Chan, A. W. Bergman, A. Levy, M. Aittala, S. D. Mello,
376 T. Karras, and G. Wetzstein. Generative novel view synthesis with 3d-aware diffusion models.
377 In *IEEE International Conference on Computer Vision (ICCV)*, October 2023.

378 [11] A. X. Chang, T. Funkhouser, L. Guibas, P. Hanrahan, Q. Huang, Z. Li, S. Savarese, M. Savva,
379 S. Song, H. Su, J. Xiao, L. Yi, and F. Yu. ShapeNet: An Information-Rich 3D Model Repository.
380 Technical Report arXiv:1512.03012 [cs.GR], Stanford University — Princeton University —
381 Toyota Technological Institute at Chicago, 2015.

382 [12] Y.-C. Cheng, H.-Y. Lee, S. Tuyakov, A. Schwing, and L. Gui. SDFusion: Multimodal 3d shape
383 completion, reconstruction, and generation. In *CVPR*, 2023.

384 [13] F. Darmon, L. Porzi, S. Rota-Bulò, and P. Koutscheder. Robust gaussian splatting. *arXiv*
385 *preprint arXiv:2404.04211*, 2024.

386 [14] M. Deitke, R. Liu, M. Wallingford, H. Ngo, O. Michel, A. Kusupati, A. Fan, C. Laforte,
387 V. Voleti, S. Y. Gadre, et al. Objaverse-xl: A universe of 10m+ 3d objects. *Advances in Neural*
388 *Information Processing Systems*, 36, 2024.

389 [15] Y. Deng, J. Yang, J. Xiang, and X. Tong. Gram: Generative radiance manifolds for 3d-aware
390 image generation. In *IEEE Computer Vision and Pattern Recognition*, 2022.

391 [16] T. Devries, M. Á. Bautista, N. Srivastava, G. W. Taylor, and J. M. Susskind. Unconstrained scene
392 generation with locally conditioned radiance fields. *2021 IEEE/CVF International Conference*
393 *on Computer Vision (ICCV)*, pages 14284–14293, 2021.

394 [17] S. A. Eslami, D. J. Rezende, F. Besse, F. Viola, A. S. Morcos, M. Garnelo, A. Ruderman,
 395 A. A. Rusu, I. Danihelka, K. Gregor, et al. Neural scene representation and rendering. *Science*,
 396 360(6394):1204–1210, 2018.

397 [18] R. Gao, A. Holynski, P. Henzler, A. Brussee, R. Martin-Brualla, P. P. Srinivasan, J. T. Barron,
 398 and B. Poole. Cat3d: Create anything in 3d with multi-view diffusion models. *Advances in
 399 Neural Information Processing Systems*, 2024.

400 [19] I. Goodfellow, J. Pouget-Abadie, M. Mirza, B. Xu, D. Warde-Farley, S. Ozair, A. Courville, and
 401 Y. Bengio. Generative adversarial nets. *Advances in neural information processing systems*, 27,
 402 2014.

403 [20] J. Gu, Q. Gao, S. Zhai, B. Chen, L. Liu, and J. Susskind. Learning controllable 3d diffusion
 404 models from single-view images. *ArXiv*, 2023.

405 [21] A. Gupta, W. Xiong, Y. Nie, I. Jones, and B. Oğuz. 3dgen: Triplane latent diffusion for textured
 406 mesh generation. *arXiv preprint arXiv:2303.05371*, 2023.

407 [22] J. Han, F. Kokkinos, and P. Torr. Vfusion3d: Learning scalable 3d generative models from
 408 video diffusion models. In *European Conference on Computer Vision*, pages 333–350. Springer,
 409 2025.

410 [23] P. Henderson and V. Ferrari. Learning single-image 3D reconstruction by generative modelling
 411 of shape, pose and shading. *International Journal of Computer Vision (IJCV)*, 2019.

412 [24] P. Henderson, C. H. Lampert, and B. Bickel. Unsupervised video prediction from a single frame
 413 by estimating 3d dynamic scene structure. *CoRR*, abs/2106.09051, 2021.

414 [25] P. Henderson, V. Tsiminaki, and C. Lampert. Leveraging 2D data to learn textured 3D mesh
 415 generation. In *IEEE Conference on Computer Vision and Pattern Recognition (CVPR)*, 2020.

416 [26] J. Ho, A. Jain, and P. Abbeel. Denoising diffusion probabilistic models. *Advances in Neural
 417 Information Processing Systems*, 33:6840–6851, 2020.

418 [27] L. Höllerin, A. Božič, N. Müller, D. Novotny, H.-Y. Tseng, C. Richardt, M. Zollhöfer, and
 419 M. Nießner. Viewdiff: 3d-consistent image generation with text-to-image models. In *Proceedings
 420 of the IEEE/CVF Conference on Computer Vision and Pattern Recognition*, 2024.

421 [28] H. Hu, Z. Zhou, V. Jampani, and S. Tulsiani. Mvd-fusion: Single-view 3d via depth-consistent
 422 multi-view generation. In *CVPR*, 2024.

423 [29] K.-H. Hui, R. Li, J. Hu, and C.-W. Fu. Neural wavelet-domain diffusion for 3d shape generation.
 424 In *SIGGRAPH Asia 2022 Conference Papers*, pages 1–9, 2022.

425 [30] A. Hyvärinen and E. Oja. Independent component analysis: algorithms and applications. *Neural
 426 networks*, 13(4-5):411–430, 2000.

427 [31] A. Jain, M. Tancik, and P. Abbeel. Putting nerf on a diet: Semantically consistent few-shot
 428 view synthesis. In *Proceedings of the IEEE/CVF International Conference on Computer Vision*,
 429 pages 5885–5894, 2021.

430 [32] J. T. Kajiya. The rendering equation. In *Proceedings of the 13th Annual Conference on
 431 Computer Graphics and Interactive Techniques, SIGGRAPH '86*, page 143–150, New York,
 432 NY, USA, 1986. Association for Computing Machinery.

433 [33] A. Karnewar, A. Vedaldi, D. Novotny, and N. Mitra. Holodiffusion: Training a 3d diffusion
 434 model using 2d images. *ArXiv*, 2023.

435 [34] B. Kerbl, G. Kopanas, T. Leimkühler, and G. Drettakis. 3d gaussian splatting for real-time
 436 radiance field rendering. *ACM Transactions on Graphics*, 42(4):1–14, 2023.

437 [35] S. W. Kim, B. Brown, K. Yin, K. Kreis, K. Schwarz, D. Li, R. Rombach, A. Torralba, and
 438 S. Fidler. Neuralfield-lmd: Scene generation with hierarchical latent diffusion models. In *IEEE
 439 Conference on Computer Vision and Pattern Recognition (CVPR)*, 2023.

440 [36] D. P. Kingma and M. Welling. Auto-encoding variational bayes. In Y. Bengio and Y. LeCun,
 441 editors, *2nd International Conference on Learning Representations, ICLR 2014, Banff, AB,
 442 Canada, April 14-16, 2014, Conference Track Proceedings*, 2014.

443 [37] X. Kong, S. Liu, X. Lyu, M. Taher, X. Qi, and A. J. Davison. Eschernet: A generative model
 444 for scalable view synthesis. *arXiv preprint arXiv:2402.03908*, 2024.

445 [38] A. R. Kosiorek, H. Strathmann, D. Zoran, P. Moreno, R. Schneider, S. Mokrá, and D. J. Rezende.
 446 Nerf-vae: A geometry aware 3d scene generative model. In M. Meila and T. Zhang, editors,
 447 *Proceedings of the 38th International Conference on Machine Learning, ICML 2021, 18-24
 448 July 2021, Virtual Event*, volume 139 of *Proceedings of Machine Learning Research*, pages
 449 5742–5752. PMLR, 2021.

450 [39] C. Lassner and M. Zollhofer. Pulsar: Efficient sphere-based neural rendering. In *Proceedings
 451 of the IEEE/CVF Conference on Computer Vision and Pattern Recognition*, pages 1440–1449,
 452 2021.

453 [40] M. Li, Y. Duan, J. Zhou, and J. Lu. Diffusion-sdf: Text-to-shape via voxelized diffusion. In
 454 *Proceedings of the IEEE Conference on Computer Vision and Pattern Recognition (CVPR)*,
 455 2023.

456 [41] C.-H. Lin, J. Gao, L. Tang, T. Takikawa, X. Zeng, X. Huang, K. Kreis, S. Fidler, M.-Y. Liu,
 457 and T.-Y. Lin. Magic3d: High-resolution text-to-3d content creation. In *IEEE Conference on
 458 Computer Vision and Pattern Recognition (CVPR)*, 2023.

459 [42] M. Liu, C. Xu, H. Jin, L. Chen, M. Varma T, Z. Xu, and H. Su. One-2-3-45: Any single image
 460 to 3d mesh in 45 seconds without per-shape optimization. *Advances in Neural Information
 461 Processing Systems*, 36, 2024.

462 [43] R. Liu, R. Wu, B. V. Hoorick, P. Tokmakov, S. Zakharov, and C. Vondrick. Zero-1-to-3:
 463 Zero-shot one image to 3d object, 2023.

464 [44] X. Liu, C. Zhou, and S. Huang. 3DGS-enhancer: Enhancing unbounded 3d gaussian splatting
 465 with view-consistent 2d diffusion priors. In *The Thirty-eighth Annual Conference on Neural
 466 Information Processing Systems*, 2024.

467 [45] Y. Liu, C. Lin, Z. Zeng, X. Long, L. Liu, T. Komura, and W. Wang. Syncdreamer: Generating
 468 multiview-consistent images from a single-view image. In *The Twelfth International Conference
 469 on Learning Representations*, 2024.

470 [46] S. Luo and W. Hu. Diffusion probabilistic models for 3d point cloud generation. *2021 IEEE/CVF
 471 Conference on Computer Vision and Pattern Recognition (CVPR)*, Jun 2021.

472 [47] L. Melas-Kyriazi, I. Laina, C. Rupprecht, N. Neverova, A. Vedaldi, O. Gafni, and F. Kokki-
 473 nos. Im-3d: Iterative multiview diffusion and reconstruction for high-quality 3d generation.
 474 *International Conference on Machine Learning*, 2024, 2024.

475 [48] B. Mildenhall, P. P. Srinivasan, M. Tancik, J. T. Barron, R. Ramamoorthi, and R. Ng. Nerf:
 476 Representing scenes as neural radiance fields for view synthesis. In *ECCV*, 2020.

477 [49] Y. Mu, X. Zuo, C. Guo, Y. Wang, J. Lu, X. Wu, S. Xu, P. Dai, Y. Yan, and L. Cheng. Gsd:
 478 View-guided gaussian splatting diffusion for 3d reconstruction, 2024.

479 [50] N. Müller, Y. Siddiqui, L. Porzi, S. R. Bulo, P. Kortschieder, and M. Nießner. Diffrrf: Rendering-
 480 guided 3d radiance field diffusion. In *Proceedings of the IEEE/CVF Conference on Computer
 481 Vision and Pattern Recognition*, pages 4328–4338, 2023.

482 [51] T. Müller, A. Evans, C. Schied, and A. Keller. Instant neural graphics primitives with a
 483 multiresolution hash encoding. *ACM Trans. Graph.*, 41(4):102:1–102:15, July 2022.

484 [52] T. Nguyen-Phuoc, C. Li, L. Theis, C. Richardt, and Y.-L. Yang. Hologan: Unsupervised learning
 485 of 3d representations from natural images. In *Proceedings of the IEEE/CVF International
 486 Conference on Computer Vision*, pages 7588–7597, 2019.

487 [53] T. Nguyen-Phuoc, C. Richardt, L. Mai, Y.-L. Yang, and N. Mitra. Blockgan: Learning 3d
 488 object-aware scene representations from unlabelled images. In *Advances in Neural Information
 489 Processing Systems 33*, Nov 2020.

490 [54] M. Niemeyer, J. T. Barron, B. Mildenhall, M. S. M. Sajjadi, A. Geiger, and N. Radwan. Regnerf:
 491 Regularizing neural radiance fields for view synthesis from sparse inputs. *2022 IEEE/CVF
 492 Conference on Computer Vision and Pattern Recognition (CVPR)*, Jun 2022.

493 [55] M. Nimier-David, D. Vicini, T. Zeltner, and W. Jakob. Mitsuba 2: A retargetable forward and
 494 inverse renderer. *Transactions on Graphics (Proceedings of SIGGRAPH Asia)*, 38(6), Dec.
 495 2019.

496 [56] M. Oquab, T. Dariset, T. Moutakanni, H. V. Vo, M. Szafraniec, V. Khalidov, P. Fernandez,
 497 D. HAZIZA, F. Massa, A. El-Nouby, M. Assran, N. Ballas, W. Galuba, R. Howes, P.-Y. Huang,
 498 S.-W. Li, I. Misra, M. Rabbat, V. Sharma, G. Synnaeve, H. Xu, H. Jegou, J. Mairal, P. Labatut,
 499 A. Joulin, and P. Bojanowski. DINOV2: Learning robust visual features without supervision.
 500 *Transactions on Machine Learning Research*, 2024. Featured Certification.

501 [57] A. Polyak, A. Zohar, A. Brown, A. Tjandra, A. Sinha, A. Lee, A. Vyas, B. Shi, C.-Y. Ma, C.-Y.
 502 Chuang, D. Yan, D. Choudhary, D. Wang, G. Sethi, G. Pang, H. Ma, I. Misra, J. Hou, J. Wang,
 503 K. Jagadeesh, K. Li, L. Zhang, M. Singh, M. Williamson, M. Le, M. Yu, M. K. Singh, P. Zhang,
 504 P. Vajda, Q. Duval, R. Girdhar, R. Sumbaly, S. S. Rambhatla, S. Tsai, S. Azadi, S. Datta, S. Chen,
 505 S. Bell, S. Ramaswamy, S. Sheynin, S. Bhattacharya, S. Motwani, T. Xu, T. Li, T. Hou, W.-N.
 506 Hsu, X. Yin, X. Dai, Y. Taigman, Y. Luo, Y.-C. Liu, Y.-C. Wu, Y. Zhao, Y. Kirstain, Z. He, Z. He,
 507 A. Pumarola, A. Thabet, A. Sanakoyeu, A. Mallya, B. Guo, B. Araya, B. Kerr, C. Wood, C. Liu,
 508 C. Peng, D. Vengertsev, E. Schonfeld, E. Blanchard, F. Juefei-Xu, F. Nord, J. Liang, J. Hoffman,
 509 J. Kohler, K. Fire, K. Sivakumar, L. Chen, L. Yu, L. Gao, M. Georgopoulos, R. Moritz, S. K.
 510 Sampson, S. Li, S. Parmeggiani, S. Fine, T. Fowler, V. Petrovic, and Y. Du. Movie gen: A cast
 511 of media foundation models, 2024.

512 [58] B. Poole, A. Jain, J. T. Barron, and B. Mildenhall. Dreamfusion: Text-to-3d using 2d diffusion.
 513 In *The Eleventh International Conference on Learning Representations*, 2023.

514 [59] A. Radford, J. W. Kim, C. Hallacy, A. Ramesh, G. Goh, S. Agarwal, G. Sastry, A. Askell,
 515 P. Mishkin, J. Clark, et al. Learning transferable visual models from natural language supervision.
 516 In *International Conference on Machine Learning*, pages 8748–8763. PMLR, 2021.

517 [60] A. Radford and K. Narasimhan. Improving language understanding by generative pre-training.
 518 OpenAI, 2018.

519 [61] J. Reizenstein, R. Shapovalov, P. Henzler, L. Sbordone, P. Labatut, and D. Novotny. Common
 520 objects in 3d: Large-scale learning and evaluation of real-life 3d category reconstruction. In
 521 *International Conference on Computer Vision*, 2021.

522 [62] D. J. Rezende, S. Mohamed, and D. Wierstra. Stochastic backpropagation and approximate
 523 inference in deep generative models. In *International conference on machine learning*, pages
 524 1278–1286. PMLR, 2014.

525 [63] B. Roessle, N. Müller, L. Porzi, S. R. Bulò, P. Kortscheder, and M. Nießner. Ganerf: Leveraging
 526 discriminators to optimize neural radiance fields. *ACM Trans. Graph.*, 42(6), nov 2023.

527 [64] R. Rombach, A. Blattmann, D. Lorenz, P. Esser, and B. Ommer. High-resolution image synthesis
 528 with latent diffusion models. In *Proceedings of the IEEE/CVF Conference on Computer Vision
 529 and Pattern Recognition (CVPR)*, pages 10684–10695, June 2022.

530 [65] K. Sargent, Z. Li, T. Shah, C. Herrmann, H.-X. Yu, Y. Zhang, E. R. Chan, D. Lagun, L. Fei-Fei,
 531 D. Sun, and J. Wu. ZeroNVS: Zero-shot 360-degree view synthesis from a single real image.
 532 *CVPR*, 2024, 2023.

533 [66] K. Schwarz, Y. Liao, M. Niemeyer, and A. Geiger. GRAF: generative radiance fields for
 534 3d-aware image synthesis. In H. Larochelle, M. Ranzato, R. Hadsell, M. Balcan, and H. Lin,
 535 editors, *Advances in Neural Information Processing Systems 33: Annual Conference on Neural
 536 Information Processing Systems 2020, NeurIPS 2020, December 6-12, 2020, virtual*, 2020.

537 [67] Y. Shen, D. Ceylan, P. Guerrero, Z. Xu, N. J. Mitra, S. Wang, and A. Frühstück. Supergaussian:
 538 Repurposing video models for 3d super resolution. In *European Conference on Computer*
 539 *Vision*, pages 215–233. Springer, 2025.

540 [68] J. R. Shue, E. R. Chan, R. Po, Z. Ankner, J. Wu, and G. Wetzstein. 3d neural field generation
 541 using triplane diffusion. *arXiv preprint arXiv:2211.16677*, 2022.

542 [69] J. Sohl-Dickstein, E. Weiss, N. Maheswaranathan, and S. Ganguli. Deep unsupervised learning
 543 using nonequilibrium thermodynamics. In F. Bach and D. Blei, editors, *Proceedings of the*
 544 *32nd International Conference on Machine Learning*, volume 37 of *Proceedings of Machine*
 545 *Learning Research*, pages 2256–2265, Lille, France, 07–09 Jul 2015. PMLR.

546 [70] J. Song, C. Meng, and S. Ermon. Denoising diffusion implicit models. In *International*
 547 *Conference on Learning Representations*, 2021.

548 [71] Y. Song, J. Sohl-Dickstein, D. P. Kingma, A. Kumar, S. Ermon, and B. Poole. Score-based
 549 generative modeling through stochastic differential equations. *arXiv preprint arXiv:2011.13456*,
 550 2020.

551 [72] Y. Song, J. Sohl-Dickstein, D. P. Kingma, A. Kumar, S. Ermon, and B. Poole. Score-based
 552 generative modeling through stochastic differential equations. In *International Conference on*
 553 *Learning Representations*, 2021.

554 [73] R. S. Sutton. The bitter lesson. <http://www.incompleteideas.net/IncIdeas/BitterLesson.html>, 2019.

556 [74] S. Szymanowicz, C. Rupprecht, and A. Vedaldi. Viewset diffusion: (0-)image-conditioned 3D
 557 generative models from 2D data. In *ICCV*, 2023.

558 [75] J. Tang, Z. Chen, X. Chen, T. Wang, G. Zeng, and Z. Liu. Lgm: Large multi-view gaussian
 559 model for high-resolution 3d content creation. *arXiv preprint arXiv:2402.05054*, 2024.

560 [76] J. Tang, J. Ren, H. Zhou, Z. Liu, and G. Zeng. Dreamgaussian: Generative gaussian splatting
 561 for efficient 3d content creation. In *The Twelfth International Conference on Learning*
 562 *Representations*, 2024.

563 [77] S. Tang, J. Chen, D. Wang, C. Tang, F. Zhang, Y. Fan, V. Chandra, Y. Furukawa, and R. Ranjan.
 564 Mvdiffusion++: A dense high-resolution multi-view diffusion model for single or sparse-view
 565 3d object reconstruction. *arXiv preprint arXiv:2402.12712*, 2024.

566 [78] A. Tewari, T. Yin, G. Cazenavette, S. Rezchikov, J. B. Tenenbaum, F. Durand, W. T. Freeman,
 567 and V. Sitzmann. Diffusion with forward models: Solving stochastic inverse problems without
 568 direct supervision. In *Thirty-seventh Conference on Neural Information Processing Systems*,
 569 2023.

570 [79] A. Vahdat, F. Williams, Z. Gojcic, O. Litany, S. Fidler, K. Kreis, et al. Lion: Latent point
 571 diffusion models for 3d shape generation. *Advances in Neural Information Processing Systems*,
 572 35:10021–10039, 2022.

573 [80] A. Van Den Oord, N. Kalchbrenner, and K. Kavukcuoglu. Pixel recurrent neural networks. In
 574 *International conference on machine learning*, pages 1747–1756. PMLR, 2016.

575 [81] A. Vaswani, N. Shazeer, N. Parmar, J. Uszkoreit, L. Jones, A. N. Gomez, L. u. Kaiser, and
 576 I. Polosukhin. Attention is all you need. In I. Guyon, U. V. Luxburg, S. Bengio, H. Wallach,
 577 R. Fergus, S. Vishwanathan, and R. Garnett, editors, *Advances in Neural Information Processing*
 578 *Systems*, volume 30. Curran Associates, Inc., 2017.

579 [82] V. Voleti, C.-H. Yao, M. Boss, A. Letts, D. Pankratz, D. Tochilkin, C. Laforte, R. Rombach, and
 580 V. Jampani. Sv3d: Novel multi-view synthesis and 3d generation from a single image using
 581 latent video diffusion. In *European Conference on Computer Vision*, pages 439–457. Springer,
 582 2025.

583 [83] H. Wang, X. Du, J. Li, R. A. Yeh, and G. Shakhnarovich. Score jacobian chaining: Lifting
 584 pretrained 2d diffusion models for 3d generation. In *Proceedings of the IEEE/CVF Conference*
 585 *on Computer Vision and Pattern Recognition*, pages 12619–12629, 2023.

586 [84] T. Wang, B. Zhang, T. Zhang, S. Gu, J. Bao, T. Baltrusaitis, J. Shen, D. Chen, F. Wen, Q. Chen,
587 and B. Guo. Rodin: A generative model for sculpting 3d digital avatars using diffusion. *ArXiv*,
588 2022.

589 [85] Z. Wang, C. Lu, Y. Wang, F. Bao, C. Li, H. Su, and J. Zhu. Prolificdreamer: High-fidelity and
590 diverse text-to-3d generation with variational score distillation. *Advances in Neural Information
591 Processing Systems*, 36, 2024.

592 [86] R. Wu, B. Mildenhall, P. Henzler, K. Park, R. Gao, D. Watson, P. P. Srinivasan, D. Verbin, J. T.
593 Barron, B. Poole, and A. Holynski. Reconfusion: 3d reconstruction with diffusion priors. In
594 *CVPR*, pages 21551–21561, 2024.

595 [87] Y. Xu, H. Tan, F. Luan, S. Bi, P. Wang, J. Li, Z. Shi, K. Sunkavalli, G. Wetzstein, Z. Xu, and
596 K. Zhang. DMV3d: Denoising multi-view diffusion using 3d large reconstruction model. In
597 *The Twelfth International Conference on Learning Representations*, 2024.

598 [88] A. Yu, V. Ye, M. Tancik, and A. Kanazawa. pixelnerf: Neural radiance fields from one or
599 few images. In *Proceedings of the IEEE/CVF Conference on Computer Vision and Pattern
600 Recognition*, pages 4578–4587, 2021.

601 [89] B. Zhang, Y. Chen, C. Wang, F. Zhao, Y. Tang, D. Chen, and B. Guo. Gaussiancube: Structuring
602 gaussian splatting using optimal transport for 3d generative modeling. In *Advances in Neural
603 Information Processing Systems (NeurIPS)*, 2024.

604 [90] J. J. Zhou, H. Gao, V. Voleti, A. Vasishta, C.-H. Yao, M. Boss, P. Torr, C. Rupprecht, and
605 V. Jampani. Stable virtual camera: Generative view synthesis with diffusion models. *arXiv
606 preprint*, 2025.

607 [91] Z. Zhou and S. Tulsiani. Sparsefusion: Distilling view-conditioned diffusion for 3d reconstruc-
608 tion. In *CVPR*, 2023.

609 **Supplementary Material**

610 We have introduced a novel probabilistic framework for 3D reconstruction that uses autoregressive
611 image generation conditioned on a iteratively updated 3D representation. By iteratively sampling
612 images consistent with the 3D representation, our approach overcomes the limitations of prior 2D
613 and 3D generative models at sampling many images, enabling state-of-the-art single-image 3D
614 reconstructions of unbounded scenes at arbitrary resolutions. In this section, we discuss limitations
615 (A)), additional details on the generative model (B)), additional results (C), 3D representation (D)
616 and pose sampling (E) used in our framework.

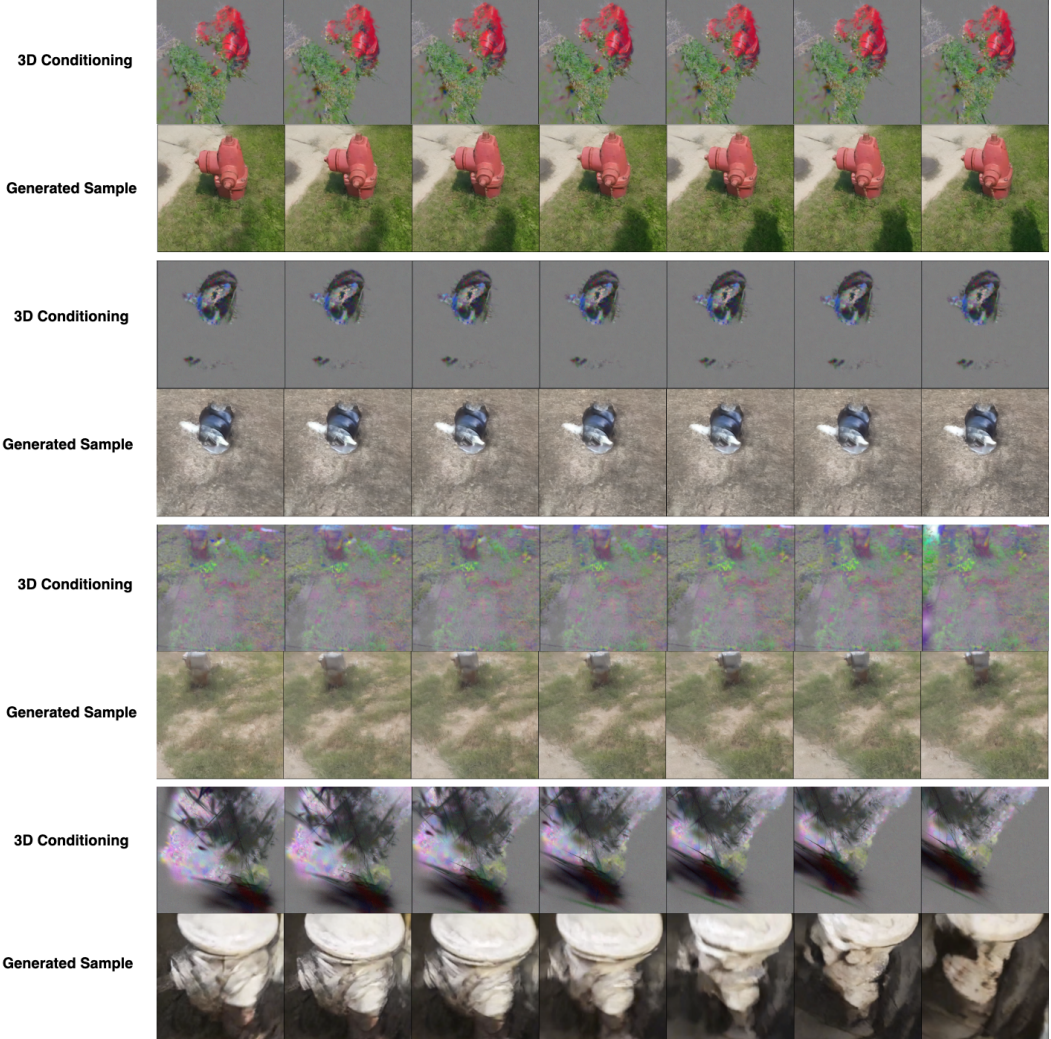


Figure 3: Visualization of a training step in our generative model. The model denoises noisy latent frames while conditioned on both input images and the 3D representation via rendered views. The process demonstrates the model’s ability to generate content that is structurally consistent with the evolving 3D representation, effectively filling in missing details.

617 **A Limitations.**

618 Our model generates 3D scenes iteratively, which enhances the fidelity of the 3D representation.
619 However, this approach incurs a trade-off in terms of generation speed, as batches must be repeatedly
620 generated by the generative model. Future work could explore the use of faster generative models
621 than diffusion models or investigate one-step prediction techniques to mitigate this issue. Another

622 limitation is that the transition from images \mathbf{x} to 3D representation \mathbf{z} occurs without priors. While this
623 allows for a clear separation between reconstruction method and 3D representation, it also means that
624 the 3D reconstruction process lacks inherent priors which often results in artifacts that are typically
625 not present in 3D-aware methods. Future research could address this by incorporating 3D-aware
626 models, to directly update 3D representation \mathbf{z}^i .

627 **B Additional details on Generative Model**

628 As described in Section 3.1, we train a latent video diffusion model conditioned on both the 3D
629 representation and the input image. During training, the model denoises sequences of 20 frames,
630 where 2D images – rendered from the 3D model – are concatenated along the channel dimension
631 with noisy latents. These are fed into the denoising UNet. The input images are processed using
632 CLIP and DINO feature extractors, and at each block of the UNet, the denoising UNet attends to
633 these features via cross-attention.
634 To enhance robustness, we apply random conditioning dropout during training: input images are
635 dropped with a probability of 0.1, 3D conditioning is dropped with a probability of 0.1, and both are
636 simultaneously dropped with a probability of 0.1. During sampling, we use classifier-free guidance
637 to control the trade-off between fidelity and diversity.

638 **C Additional Qualitative Results**

639 We visualize random training steps in Figure 3, where the model is tasked with denoising noisy latents
640 while conditioned on both input images and the 3D representation. The visualization highlights
641 how the model learns to predict content that is structurally consistent with the 3D representation,
642 successfully inferring missing details.

643 **D Additional Details on 3D Representation and Rendering**

644 Though our framework is independent of 3D representation, for all our experiments, we use 3D
645 Gaussian Splatting [34] as the underlying scene representation. The 3D Gaussians are initialized using
646 a depth estimator applied to the generated video frames, extracting a 3D point cloud. This approach
647 aligns with prior methods such as CAT3D [18], ensuring a structured and scalable representation of
648 the scene.

649 **E Camera Pose Sampling**

650 The camera poses where new images are being generated are sampled from $P_\lambda(\mathbf{c}^g \mid \mathbf{c}^c)$ which we
651 carefully design so that that P_θ can easily generate consistent images. In practice, this involves:
652 (i) Sampling views near previously generated ones rather than those on the opposite side of the
653 input image, as the latter introduces high uncertainty due to unobserved regions. This is done
654 autoregressively, using the previous endpoint as the new starting point. (ii) Sampling camera
655 trajectories that resemble those in the CO3D dataset, which the model was trained on. For the latter,
656 we also create zoom-out and zoom-in effects, by estimating world center and adding or subtracting
657 small amounts of distances to each camera pose.

658 **NeurIPS Paper Checklist**

659 The checklist is designed to encourage best practices for responsible machine learning research,
660 addressing issues of reproducibility, transparency, research ethics, and societal impact. Do not remove
661 the checklist: **The papers not including the checklist will be desk rejected.** The checklist should
662 follow the references and follow the (optional) supplemental material. The checklist does NOT count
663 towards the page limit.

664 Please read the checklist guidelines carefully for information on how to answer these questions. For
665 each question in the checklist:

666 • You should answer **[Yes]** , **[No]** , or **[NA]** .
667 • **[NA]** means either that the question is Not Applicable for that particular paper or the
668 relevant information is Not Available.
669 • Please provide a short (1–2 sentence) justification right after your answer (even for NA).

670 **The checklist answers are an integral part of your paper submission.** They are visible to the
671 reviewers, area chairs, senior area chairs, and ethics reviewers. You will be asked to also include it
672 (after eventual revisions) with the final version of your paper, and its final version will be published
673 with the paper.

674 The reviewers of your paper will be asked to use the checklist as one of the factors in their evaluation.
675 While "**[Yes]**" is generally preferable to "**[No]**", it is perfectly acceptable to answer "**[No]**" provided a
676 proper justification is given (e.g., "error bars are not reported because it would be too computationally
677 expensive" or "we were unable to find the license for the dataset we used"). In general, answering
678 "**[No]**" or "**[NA]**" is not grounds for rejection. While the questions are phrased in a binary way, we
679 acknowledge that the true answer is often more nuanced, so please just use your best judgment and
680 write a justification to elaborate. All supporting evidence can appear either in the main paper or the
681 supplemental material, provided in appendix. If you answer **[Yes]** to a question, in the justification
682 please point to the section(s) where related material for the question can be found.

683 **IMPORTANT**, please:

684 • **Delete this instruction block, but keep the section heading "NeurIPS Paper Checklist",**
685 • **Keep the checklist subsection headings, questions/answers and guidelines below.**
686 • **Do not modify the questions and only use the provided macros for your answers.**

687 **1. Claims**

688 Question: Do the main claims made in the abstract and introduction accurately reflect the
689 paper's contributions and scope?

690 Answer: **[Yes]**

691 Justification: WRITE HERE

692 Guidelines:

693 • The answer NA means that the abstract and introduction do not include the claims
694 made in the paper.
695 • The abstract and/or introduction should clearly state the claims made, including the
696 contributions made in the paper and important assumptions and limitations. A No or
697 NA answer to this question will not be perceived well by the reviewers.
698 • The claims made should match theoretical and experimental results, and reflect how
699 much the results can be expected to generalize to other settings.
700 • It is fine to include aspirational goals as motivation as long as it is clear that these goals
701 are not attained by the paper.

702 **2. Limitations**

703 Question: Does the paper discuss the limitations of the work performed by the authors?

704 Answer: **[Yes]**

705 Justification: At the end of the paper.

706 Guidelines:

- 707 • The answer NA means that the paper has no limitation while the answer No means that
708 the paper has limitations, but those are not discussed in the paper.
- 709 • The authors are encouraged to create a separate "Limitations" section in their paper.
- 710 • The paper should point out any strong assumptions and how robust the results are to
711 violations of these assumptions (e.g., independence assumptions, noiseless settings,
712 model well-specification, asymptotic approximations only holding locally). The authors
713 should reflect on how these assumptions might be violated in practice and what the
714 implications would be.
- 715 • The authors should reflect on the scope of the claims made, e.g., if the approach was
716 only tested on a few datasets or with a few runs. In general, empirical results often
717 depend on implicit assumptions, which should be articulated.
- 718 • The authors should reflect on the factors that influence the performance of the approach.
719 For example, a facial recognition algorithm may perform poorly when image resolution
720 is low or images are taken in low lighting. Or a speech-to-text system might not be
721 used reliably to provide closed captions for online lectures because it fails to handle
722 technical jargon.
- 723 • The authors should discuss the computational efficiency of the proposed algorithms
724 and how they scale with dataset size.
- 725 • If applicable, the authors should discuss possible limitations of their approach to
726 address problems of privacy and fairness.
- 727 • While the authors might fear that complete honesty about limitations might be used by
728 reviewers as grounds for rejection, a worse outcome might be that reviewers discover
729 limitations that aren't acknowledged in the paper. The authors should use their best
730 judgment and recognize that individual actions in favor of transparency play an impor-
731 tant role in developing norms that preserve the integrity of the community. Reviewers
732 will be specifically instructed to not penalize honesty concerning limitations.

733 **3. Theory assumptions and proofs**

734 Question: For each theoretical result, does the paper provide the full set of assumptions and
735 a complete (and correct) proof?

736 Answer: [NA]

737 Justification: No theoretical results

738 Guidelines:

- 739 • The answer NA means that the paper does not include theoretical results.
- 740 • All the theorems, formulas, and proofs in the paper should be numbered and cross-
741 referenced.
- 742 • All assumptions should be clearly stated or referenced in the statement of any theorems.
- 743 • The proofs can either appear in the main paper or the supplemental material, but if
744 they appear in the supplemental material, the authors are encouraged to provide a short
745 proof sketch to provide intuition.
- 746 • Inversely, any informal proof provided in the core of the paper should be complemented
747 by formal proofs provided in appendix or supplemental material.
- 748 • Theorems and Lemmas that the proof relies upon should be properly referenced.

749 **4. Experimental result reproducibility**

750 Question: Does the paper fully disclose all the information needed to reproduce the main ex-
751 perimental results of the paper to the extent that it affects the main claims and/or conclusions
752 of the paper (regardless of whether the code and data are provided or not)?

753 Answer: [Yes]

754 Justification: Details provided in the method and supplementary

755 Guidelines:

- 756 • The answer NA means that the paper does not include experiments.

- 757 • If the paper includes experiments, a No answer to this question will not be perceived
 758 well by the reviewers: Making the paper reproducible is important, regardless of
 759 whether the code and data are provided or not.
- 760 • If the contribution is a dataset and/or model, the authors should describe the steps taken
 761 to make their results reproducible or verifiable.
- 762 • Depending on the contribution, reproducibility can be accomplished in various ways.
 763 For example, if the contribution is a novel architecture, describing the architecture fully
 764 might suffice, or if the contribution is a specific model and empirical evaluation, it may
 765 be necessary to either make it possible for others to replicate the model with the same
 766 dataset, or provide access to the model. In general, releasing code and data is often
 767 one good way to accomplish this, but reproducibility can also be provided via detailed
 768 instructions for how to replicate the results, access to a hosted model (e.g., in the case
 769 of a large language model), releasing of a model checkpoint, or other means that are
 770 appropriate to the research performed.
- 771 • While NeurIPS does not require releasing code, the conference does require all submis-
 772 sions to provide some reasonable avenue for reproducibility, which may depend on the
 773 nature of the contribution. For example
 - 774 (a) If the contribution is primarily a new algorithm, the paper should make it clear how
 775 to reproduce that algorithm.
 - 776 (b) If the contribution is primarily a new model architecture, the paper should describe
 777 the architecture clearly and fully.
 - 778 (c) If the contribution is a new model (e.g., a large language model), then there should
 779 either be a way to access this model for reproducing the results or a way to reproduce
 780 the model (e.g., with an open-source dataset or instructions for how to construct
 781 the dataset).
 - 782 (d) We recognize that reproducibility may be tricky in some cases, in which case
 783 authors are welcome to describe the particular way they provide for reproducibility.
 784 In the case of closed-source models, it may be that access to the model is limited in
 785 some way (e.g., to registered users), but it should be possible for other researchers
 786 to have some path to reproducing or verifying the results.

787 5. Open access to data and code

788 Question: Does the paper provide open access to the data and code, with sufficient instruc-
 789 tions to faithfully reproduce the main experimental results, as described in supplemental
 790 material?

791 Answer: **[Yes]**

792 Justification: Will be made available post publication.

793 Guidelines:

- 794 • The answer NA means that paper does not include experiments requiring code.
- 795 • Please see the NeurIPS code and data submission guidelines (<https://nips.cc/public/guides/CodeSubmissionPolicy>) for more details.
- 796 • While we encourage the release of code and data, we understand that this might not be
 797 possible, so “No” is an acceptable answer. Papers cannot be rejected simply for not
 798 including code, unless this is central to the contribution (e.g., for a new open-source
 799 benchmark).
- 800 • The instructions should contain the exact command and environment needed to run to
 801 reproduce the results. See the NeurIPS code and data submission guidelines (<https://nips.cc/public/guides/CodeSubmissionPolicy>) for more details.
- 802 • The authors should provide instructions on data access and preparation, including how
 803 to access the raw data, preprocessed data, intermediate data, and generated data, etc.
- 804 • The authors should provide scripts to reproduce all experimental results for the new
 805 proposed method and baselines. If only a subset of experiments are reproducible, they
 806 should state which ones are omitted from the script and why.
- 807 • At submission time, to preserve anonymity, the authors should release anonymized
 808 versions (if applicable).

811 • Providing as much information as possible in supplemental material (appended to the
812 paper) is recommended, but including URLs to data and code is permitted.

813 **6. Experimental setting/details**

814 Question: Does the paper specify all the training and test details (e.g., data splits, hyper-
815 parameters, how they were chosen, type of optimizer, etc.) necessary to understand the
816 results?

817 Answer: **[Yes]**

818 Justification: Provided in method, supplementary and post publication release.

819 Guidelines:

820 • The answer NA means that the paper does not include experiments.
821 • The experimental setting should be presented in the core of the paper to a level of detail
822 that is necessary to appreciate the results and make sense of them.
823 • The full details can be provided either with the code, in appendix, or as supplemental
824 material.

825 **7. Experiment statistical significance**

826 Question: Does the paper report error bars suitably and correctly defined or other appropriate
827 information about the statistical significance of the experiments?

828 Answer: **[No]**

829 Justification:

830 Guidelines:

831 • The answer NA means that the paper does not include experiments.
832 • The authors should answer "Yes" if the results are accompanied by error bars, confi-
833 dence intervals, or statistical significance tests, at least for the experiments that support
834 the main claims of the paper.
835 • The factors of variability that the error bars are capturing should be clearly stated (for
836 example, train/test split, initialization, random drawing of some parameter, or overall
837 run with given experimental conditions).
838 • The method for calculating the error bars should be explained (closed form formula,
839 call to a library function, bootstrap, etc.)
840 • The assumptions made should be given (e.g., Normally distributed errors).
841 • It should be clear whether the error bar is the standard deviation or the standard error
842 of the mean.
843 • It is OK to report 1-sigma error bars, but one should state it. The authors should
844 preferably report a 2-sigma error bar than state that they have a 96% CI, if the hypothesis
845 of Normality of errors is not verified.
846 • For asymmetric distributions, the authors should be careful not to show in tables or
847 figures symmetric error bars that would yield results that are out of range (e.g. negative
848 error rates).
849 • If error bars are reported in tables or plots, The authors should explain in the text how
850 they were calculated and reference the corresponding figures or tables in the text.

851 **8. Experiments compute resources**

852 Question: For each experiment, does the paper provide sufficient information on the com-
853 puter resources (type of compute workers, memory, time of execution) needed to reproduce
854 the experiments?

855 Answer: **[Yes]**

856 Justification: Yes in supplementary

857 Guidelines:

858 • The answer NA means that the paper does not include experiments.
859 • The paper should indicate the type of compute workers CPU or GPU, internal cluster,
860 or cloud provider, including relevant memory and storage.

861 • The paper should provide the amount of compute required for each of the individual
862 experimental runs as well as estimate the total compute.
863 • The paper should disclose whether the full research project required more compute
864 than the experiments reported in the paper (e.g., preliminary or failed experiments that
865 didn't make it into the paper).

866 **9. Code of ethics**

867 Question: Does the research conducted in the paper conform, in every respect, with the
868 NeurIPS Code of Ethics <https://neurips.cc/public/EthicsGuidelines>?

869 Answer: [Yes]

870 Justification:

871 Guidelines:

872 • The answer NA means that the authors have not reviewed the NeurIPS Code of Ethics.
873 • If the authors answer No, they should explain the special circumstances that require a
874 deviation from the Code of Ethics.
875 • The authors should make sure to preserve anonymity (e.g., if there is a special consider-
876 ation due to laws or regulations in their jurisdiction).

877 **10. Broader impacts**

878 Question: Does the paper discuss both potential positive societal impacts and negative
879 societal impacts of the work performed?

880 Answer: [NA]

881 Justification: We do not foresee any direct societal impact resulting from this work. While
882 the proposed method involves image generation and 3D reconstruction, it is not designed
883 for or applied to human subjects. Although, in theory, similar techniques could be adapted
884 for misuse (e.g. in generating deepfakes), our work does not directly enable or target such
885 applications.

886 Guidelines:

887 • The answer NA means that there is no societal impact of the work performed.
888 • If the authors answer NA or No, they should explain why their work has no societal
889 impact or why the paper does not address societal impact.
890 • Examples of negative societal impacts include potential malicious or unintended uses
891 (e.g., disinformation, generating fake profiles, surveillance), fairness considerations
892 (e.g., deployment of technologies that could make decisions that unfairly impact specific
893 groups), privacy considerations, and security considerations.
894 • The conference expects that many papers will be foundational research and not tied
895 to particular applications, let alone deployments. However, if there is a direct path to
896 any negative applications, the authors should point it out. For example, it is legitimate
897 to point out that an improvement in the quality of generative models could be used to
898 generate deepfakes for disinformation. On the other hand, it is not needed to point out
899 that a generic algorithm for optimizing neural networks could enable people to train
900 models that generate Deepfakes faster.
901 • The authors should consider possible harms that could arise when the technology is
902 being used as intended and functioning correctly, harms that could arise when the
903 technology is being used as intended but gives incorrect results, and harms following
904 from (intentional or unintentional) misuse of the technology.
905 • If there are negative societal impacts, the authors could also discuss possible mitigation
906 strategies (e.g., gated release of models, providing defenses in addition to attacks,
907 mechanisms for monitoring misuse, mechanisms to monitor how a system learns from
908 feedback over time, improving the efficiency and accessibility of ML).

909 **11. Safeguards**

910 Question: Does the paper describe safeguards that have been put in place for responsible
911 release of data or models that have a high risk for misuse (e.g., pretrained language models,
912 image generators, or scraped datasets)?

913 Answer: [NA]

914 Justification: See above

915 Guidelines:

- 916 • The answer NA means that the paper poses no such risks.
- 917 • Released models that have a high risk for misuse or dual-use should be released with
- 918 necessary safeguards to allow for controlled use of the model, for example by requiring
- 919 that users adhere to usage guidelines or restrictions to access the model or implementing
- 920 safety filters.
- 921 • Datasets that have been scraped from the Internet could pose safety risks. The authors
- 922 should describe how they avoided releasing unsafe images.
- 923 • We recognize that providing effective safeguards is challenging, and many papers do
- 924 not require this, but we encourage authors to take this into account and make a best
- 925 faith effort.

926 12. Licenses for existing assets

927 Question: Are the creators or original owners of assets (e.g., code, data, models), used in
928 the paper, properly credited and are the license and terms of use explicitly mentioned and
929 properly respected?

930 Answer: [Yes]

931 Justification: We cite all used datasets and followed their licence.

932 Guidelines:

- 933 • The answer NA means that the paper does not use existing assets.
- 934 • The authors should cite the original paper that produced the code package or dataset.
- 935 • The authors should state which version of the asset is used and, if possible, include a
- 936 URL.
- 937 • The name of the license (e.g., CC-BY 4.0) should be included for each asset.
- 938 • For scraped data from a particular source (e.g., website), the copyright and terms of
- 939 service of that source should be provided.
- 940 • If assets are released, the license, copyright information, and terms of use in the
- 941 package should be provided. For popular datasets, paperswithcode.com/datasets
- 942 has curated licenses for some datasets. Their licensing guide can help determine the
- 943 license of a dataset.
- 944 • For existing datasets that are re-packaged, both the original license and the license of
- 945 the derived asset (if it has changed) should be provided.
- 946 • If this information is not available online, the authors are encouraged to reach out to
- 947 the asset's creators.

948 13. New assets

949 Question: Are new assets introduced in the paper well documented and is the documentation
950 provided alongside the assets?

951 Answer: [NA]

952 Justification:

953 Guidelines:

- 954 • The answer NA means that the paper does not release new assets.
- 955 • Researchers should communicate the details of the dataset/code/model as part of their
- 956 submissions via structured templates. This includes details about training, license,
- 957 limitations, etc.
- 958 • The paper should discuss whether and how consent was obtained from people whose
- 959 asset is used.
- 960 • At submission time, remember to anonymize your assets (if applicable). You can either
- 961 create an anonymized URL or include an anonymized zip file.

962 14. Crowdsourcing and research with human subjects

963 Question: For crowdsourcing experiments and research with human subjects, does the paper
964 include the full text of instructions given to participants and screenshots, if applicable, as
965 well as details about compensation (if any)?

966 Answer: [NA]

967 Justification:

968 Guidelines:

- The answer NA means that the paper does not involve crowdsourcing nor research with human subjects.
- Including this information in the supplemental material is fine, but if the main contribution of the paper involves human subjects, then as much detail as possible should be included in the main paper.
- According to the NeurIPS Code of Ethics, workers involved in data collection, curation, or other labor should be paid at least the minimum wage in the country of the data collector.

15. Institutional review board (IRB) approvals or equivalent for research with human subjects

979 Question: Does the paper describe potential risks incurred by study participants, whether
980 such risks were disclosed to the subjects, and whether Institutional Review Board (IRB)
981 approvals (or an equivalent approval/review based on the requirements of your country or
982 institution) were obtained?

983 Answer: [NA]

984 Justification:

985 Guidelines:

- The answer NA means that the paper does not involve crowdsourcing nor research with human subjects.
- Depending on the country in which research is conducted, IRB approval (or equivalent) may be required for any human subjects research. If you obtained IRB approval, you should clearly state this in the paper.
- We recognize that the procedures for this may vary significantly between institutions and locations, and we expect authors to adhere to the NeurIPS Code of Ethics and the guidelines for their institution.
- For initial submissions, do not include any information that would break anonymity (if applicable), such as the institution conducting the review.

16. Declaration of LLM usage

997 Question: Does the paper describe the usage of LLMs if it is an important, original, or
998 non-standard component of the core methods in this research? Note that if the LLM is used
999 only for writing, editing, or formatting purposes and does not impact the core methodology,
1000 scientific rigorousness, or originality of the research, declaration is not required.

1001 Answer: [NA]

1002 Justification:

1003 Guidelines:

- The answer NA means that the core method development in this research does not involve LLMs as any important, original, or non-standard components.
- Please refer to our LLM policy (<https://neurips.cc/Conferences/2025/LLM>) for what should or should not be described.